Original Research

Comparison of T_1 and T_2 Metabolite Relaxation Times in Glioma and Normal Brain at 3T

Yan Li, MD, MS,[1,2]* Radhika Srinivasan, PhD,[2] Helene Ratiney, PhD,[3] Ying Lu, PhD,[1,2] Susan M. Chang, MD,[4] and Sarah J. Nelson, PhD[1,2,5]

Purpose: To measure T_1 and T_2 relaxation times of metabolites in glioma patients at 3T and to investigate how these values influence the observed metabolite levels.

Materials and Methods: A total of 23 patients with gliomas and 10 volunteers were studied with single-voxel two-dimensional (2D) J-resolved point-resolved spectral selection (PRESS) using a 3T MR scanner. Voxels were chosen in normal appearing white matter (WM) and in regions of tumor. The T_1 and T_2 of choline containing compounds (Cho), creatine (Cr), and N-acetyl aspartate (NAA) were estimated.

Results: Metabolite T_1 relaxation values in gliomas were not significantly different from values in normal WM. The T_2 of Cho and Cr were statistically significantly longer for grade 4 gliomas than for normal WM but the T_2 of NAA was similar. These differences were large enough to impact the corrections of metabolite levels for relaxation times with tumor grade in terms of metabolite ratios ($P < 0.001$).

Conclusion: The differential increase in T_2 for Cho and Cr relative to NAA means that the ratios of Cho/NAA and Cr/NAA are higher in tumor at longer echo times (TEs) relative to values in normal appearing brain. Having this information may be useful in defining the acquisition parameters for optimizing contrast between tumor and normal tissue in MR spectroscopic imaging (MRSI) data, in which limited time is available and only one TE can be used.

Key Words: relaxation times; glioma; 3T; Cho; Cr; NAA
J. Magn. Reson. Imaging 2008;28:342–350.

GLIOMAS ACCOUNT FOR THE MAJORITY of primary brain tumors and vary from benign to malignant. Among all the gliomas, glioblastoma multiforme (GBM) is both the most common and the most malignant, with a relatively poor prognosis. Proton magnetic resonance spectroscopy (^{1}H-MRS) is a powerful noninvasive tool that has been used for the assessment of metabolites in gliomas and the biochemical profiles of brain tumors have been widely studied (1–4). A general marker of brain tumors is the elevation of choline-containing compounds (Cho), which is thought to be due to increased cell density and membrane turnover in neoplasms, and the reduction of the neural marker N-acetyl aspartate (NAA). The availability of higher field strength MR scanners and multichannel radio frequency coils offer the potential of higher signal-to-noise ratio (SNR) and better spectral resolution (5) that can be used to either shorten acquisition time, decrease spatial resolution, or improve detection of other brain metabolites; such as, glutamate (Glu), a main excitatory neurotransmitter; glutamine (Gln), which acts as a detoxifier; and myo-inositol (mI), which is predominantly located within astrocytes.

In planning the data acquisition parameters for using MR spectroscopic imaging (MRSI) to determine the spatial extent of tumor vs. normal brain tissue, it is important to consider how to select values that will emphasize the contrast between metabolites in the different regions. Because of the restrictions on clinical scan time, the repetition time (TR) for acquiring MRSI data is often set at one to two seconds and it is usually only possible to acquire data with a single echo time (TE). In deciding which TE is most appropriate for a particular data acquisition it is critical to consider the differences in metabolite intensities caused by the effects of T_1 and T_2 relaxation times, as well as the changes in metabolite concentrations associated with pathology. Previous studies have reported a difference in T_2 relaxation time between tumor and normal tissues in brain at 1.5T (6,7), but the values reported were variable and there is no literature about the T_2 relaxation times in brain tumors at 3T.

The purpose of this study was to use a single-voxel point-resolved spectral selection (PRESS) sequence with an eight-channel phased array coil at 3T, to measure the longitudinal and transverse relaxation times of Cho, creatine (Cr), and NAA within anatomic lesions corresponding to grade 3 and grade 4 gliomas and to compare them with white matter (WM) or normal-ap-

[1]University of California, San Francisco/University of California, Berkeley (UCSF/UCB) Joint Graduate Group in Bioengineering, San Francisco, California, USA.
[2]Department of Radiology, University of California, San Francisco, San Francisco, California, USA.
[3]Centre de Recherche et d'Applications en Traitement de l'Image et du Signal–Lyon Résonance Magnétique Nucléaire (CREATIS-LRMN), Centre National de la Recherche Scientifique (CNRS) Unité Mixte de Recherche (UMR) 5220, Université Claude Bernard Lyon 1, Lyon, France.
[4]Department of Neurological Surgery, University of California, San Francisco, San Francisco, California, USA.
[5]Program in Bioengineering, University of California, San Francisco, San Francisco, California, USA.
Contract Grant Sponsor: National Institutes of Health (NIH); Contract grant numbers: RO1 CA59880, ITL-BIO 04-10148.
Presented in part at the 14th Annual Meeting of ISMRM, Seattle, WA, USA, 2006.
*Address reprint requests to: Y.L., UCSF Radiology, Box 2532, QB3/Byers Hall, Suite 303, 1700 4th Street, San Francisco, CA 94143-2532, USA. E-mail: yan.li@radiology.ucsf.edu
Received November 27, 2007; Accepted April 28, 2008.
DOI 10.1002/jmri.21453
Published online in Wiley InterScience (www.interscience.wiley.com).

pearing WM (NAWM). Because the data acquisition method that was used for this study employed two dimensional (2D) J-resolved spectroscopy, it also allowed the separation of J-coupling information from the chemical shift and improved distinction between Glu and Gln in the TE-averaged spectra by averaging across the different TEs (8). The data were used to compare estimates of metabolite levels in tumor vs. NAWM, as well as evaluating the differentials in Cho, Cr, and NAA, with and without corrections for relaxation times.

MATERIALS AND METHODS

Study Population

A total of 10 volunteers (four males and six females, median age = 28 years) and 23 patients (11 males and 12 females, median age = 44 years) with gliomas at different clinical stages were studied. Tumors were graded by histological examination of tissue samples obtained during biopsy or surgical resection. Of all the patients, there were two grade 2 oligodendrogliomas, five grade 3 (two oligodendrogliomas, and three anaplastic astrocytomas), 15 grade 4 (GBM) patients, and one oligodendroglioma with unknown grade.

Data Acquisition

All the empirical data were acquired using an eight-channel phased array coil on a 3T GE Signa scanner running the Excite software package (GE Healthcare Technologies, Waukesha, WI, USA). The MR scans included the acquisition of both anatomic and spectral data.

Anatomical MR images comprised T_1-weighted sagittal scout images (TR/TE = 70 msec/2 msec), axial fluid attenuated inversion recovery (FLAIR) (TR/TE/TI = 10,002 msec/121 msec/2200 msec) and T_1-weighted spoiled gradient echo (SPGR) images (TR/TE = 26 msec/3 msec).

All spectra were acquired using 2D J-resolved techniques. For T_2 studies and metabolite levels, 2D J-resolved PRESS data were obtained using 64 steps with a time increment of 2.5 msec starting at TE = 35 msec (8). With a TR of two seconds and the number of excitations (NEX) = 2, the total acquisition time was approximately five minutes. For T_1 studies, TE-averaged PRESS data was obtained with 16 steps and a time increment of 10 msec at TR = 1 second with NEX = 4, TR = 2 seconds with NEX = 4, and TR = 8 seconds with NEX = 2, respectively (8,9). The spectral data were acquired with number of spectral points = 2048 and spectral width = 5000 Hz. To obtain estimates of coil sensitivities for the combination of the eight-channel data, unsuppressed water spectra were acquired with TE = 35 msec with each of the PRESS spectra.

The 8-cc single voxels were located within WM, NAWM, or regions of tumor for participants. The volume of interest (VOI) from volunteers was localized in the parietal WM. The NAWM in patients was positioned as far as possible from the lesions and included four parietal NAWM voxels and six frontal NAWM voxels. The tumor regions were defined by T_2 hyperintensity from T_2 FLAIR images and positioned to cover as much of the lesion as possible. The number and regions of interest (ROI) investigated for each patient in the T_2 studies were shown as follows: four patients (NAWM only), six patients (NAWM and one tumor voxel), and nine patients (one tumor voxel only). Due to long acquisition times to measure T_1 values of metabolites, a relatively small number of patients was involved in the study and these patients varied from low grade gliomas to high grade gliomas.

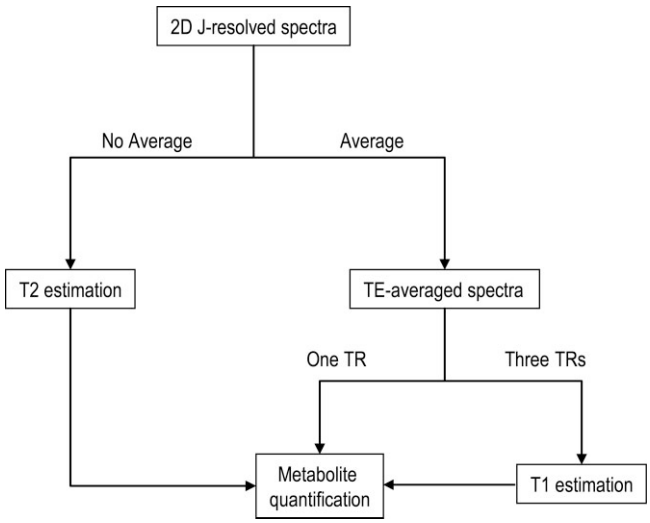

Figure 1. Scheme of the procedure for data postprocessing.

Data Processing

Postprocessing was applied on a Sun workstation (Fig. 1). The time domain data were extracted from the raw files using the SAGE software package™ (General Electric, Milwaukee, WI, USA) which is based on the IDL software package (Research Systems, Inc., Boulder, CO, USA). An internal water reference was used for phase and frequency correction, and 4-Hz Lorentzian apodization was applied in the F_2 dimension. Eight-channel data were combined in the time-domain using the unsuppressed water signal (10). Spectra were then zero-filled and processed with a fast Fourier transform (FFT). The TE-averaged free induction decay (FID) was generated by averaging the different TEs and metabolite quantification was performed without any spectral apodization or zero-filling.

Metabolite T_1 and T_2 Estimation

To increase the SNR and the accuracy of the T_2 calculation, data for each echo-time were averaged with the one before and the one after in the t_1 dimension and then Fourier-transformed in the t_2 dimension. The peak heights of Cho at 3.22 ppm, Cr-CH_3 at 3.02 ppm, and NAA at 2.02 ppm were extracted from the spectra with TE from 57.5 msec to 190 msec, a total of 54 spectra, to reduce the contamination of macromolecules and/or J-coupled multiplets, and fitted to a single exponential function. Only the T_2 fits with variances of the fit residue smaller than 10% were included in the analysis.

T_1 relaxation times were calculated from data partial saturation using a two-parameter least-squares fitting routine to the equation $S/S_0 = 1 - 2\exp[-(TR - TE/2)/T_1] + \exp(-TR/T_1)$ (11), where S is the signal intensity acquired at three different TRs, S_0 is the fully relaxed signal intensity, and the effective TE of the TE-averaged spectra for T_1 acquisition is 110 msec. The signal intensities of Cho, Cr, and NAA were normalized for the number of acquisitions that were obtained before T_1 fitting.

Estimation of Differences in Metabolite Levels

To estimate metabolite levels, the combined data were averaged in the t_1 domain before zero filling and then quantified using the LCModel package (12) and the quantitation based on quantum estimation (QUEST) quantitation algorithm (13) in the Magnetic Resonance User Interface (MRUI) spectrum analysis program.

An in vitro basis set of individual metabolites, consisting of NAA, Glu, Gln, Cr, Cho, and mI, was prepared for LCModel. The fitting was performed between 3.85 ppm and 1.8 ppm to minimize spectral artifact from lipid. Metabolite concentrations included in the analysis were those with relative Cramér-Rao lower bounds (CRLB) lower than 5% for Cho, Cr, and NAA, and 20% for mI and Glu.

For QUEST, the signals were analyzed in the time domain. To minimize the incorporation of large broad baseline components, the first data point of the FID was excluded and the first 20 points were weighted by a quarter-wave sinusoid (14). A Hankel Lanczos singular value decomposition (HLSVD) filter was applied to remove the residual water from the spectra (15). Metabolic signals for the basis set were generated using GAMMA simulations (16) with prior knowledge of chemical shift and J-coupling (17). Due to known differences in T_2 relaxation times between two singlets of Cr peak, Cr-CH_2 and Cr-CH_3 are separated into two spectra in the basis set. The selection criteria for QUEST estimates were defined by the output parameters from the QUEST analysis, namely a CRLB smaller than 20% and additional common damping factor smaller than 12 Hz. The calibration factors for both methods were obtained from a standard GE MRS head (HD) phantom (12.5 mM NAA, 10 mM Cr, 3 mM Cho, 12.5 mM Glu, 7.5 mM mI and 5 mM lactate) and 50 mM NAA only phantom (50 mM phosphate buffer, pH 7.2) and were applied in all of the data sets.

To estimate the T_2 values on the effective separation of Glu and Gln in the TE-averaged spectra, the spectra were created with 2048 spectral points, spectral width = 5000 Hz, and TE values starting at 35 msec in either 128 steps of 2.5 msec or 64 steps of 2.5 msec. To approximate the effects of transverse relaxation time and inhomogeneities for the in vivo spectra for Glu and Gln, the time data were multiplied by a factor, $e^{-t_1/T_2}e^{-t_2/T_2^*}$, where t_1 is the TE and t_2 is the total sampling time. T_2^* was set to 50 msec, which was estimated from the mean linewidth of metabolites (5), and a simple monoexponential decay was applied to the data with T_2 values of 100 msec, 150 msec, and 300 msec, respectively. A 4-Hz Lorentzian apodization, zero-filling, and Fourier transform were applied and the spectra were averaged in the t_1 domain. Figure 2 shows the TE-averaged spectra of Glu and Gln that were simulated using this approach. The efficacy of separation for C4 protons of Glu and Gln in TE-averaged spectra was the same for different T_2 values but the signal intensities of Gln depended on the T_2 values. This meant that the signals from the C4 protons of Gln were not fully cancelled in the simulation, but they were clearly separated from the C4 protons of Glu due to the difference in chemical shift being 0.1 ppm.

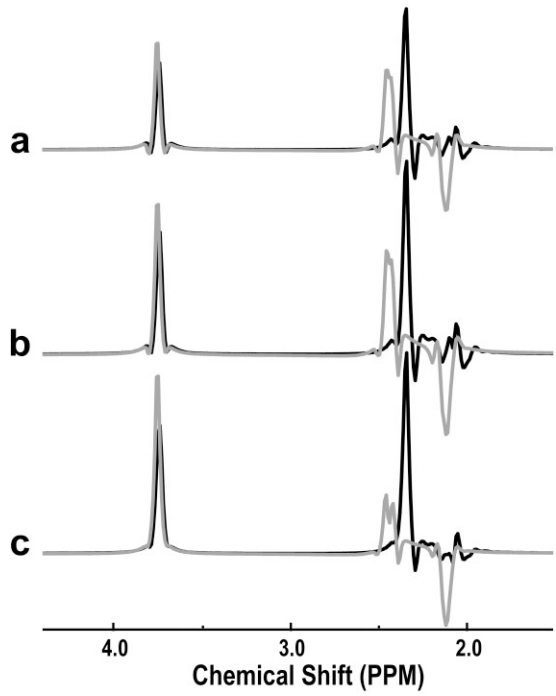

Figure 2. Simulation of TE-averaged PRESS spectra of Glu (black) and Gln (gray) with different T_2 relaxation times. TE-averaged PRESS spectra were simulated with 64 steps and T_2 of 100 msec (**a**), 64 steps and T_2 of 150 msec (**b**), and 128 steps and T_2 of 300 msec (**c**).

Corrections of Metabolite Levels for Relaxation Times

The metabolite levels were corrected for transverse and longitudinal relaxation times using the values estimated from the empirical data. T_2 correction was applied for levels of Cho, Cr, and NAA by multiplying LCModel concentrations and QUEST parameter estimates by a factor of $f_{TE} = \exp[TE \cdot (1/T_{2vivo} - 1/T_{2vitro})]$, respectively, while the effective TE of the TE-averaged spectra for T_2 acquisition was 113.75 msec, and T_1 correction factor was $f_{TR} = [1 - \exp(-TR/T_{1vitro})]/[1 - \exp(-TR/T_{1vivo})]$. for Cho, Cr, and NAA. Since the metabolite signals used as a basis for QUEST were ideally simulated without any effect of T_1 and T_2, the calibration factor only required a calculation of the in vivo T_1 and T_2 values.

Voxel Content Analysis

For the empirical data, the spectral data were referenced to the 3D SPGR image by assuming that there

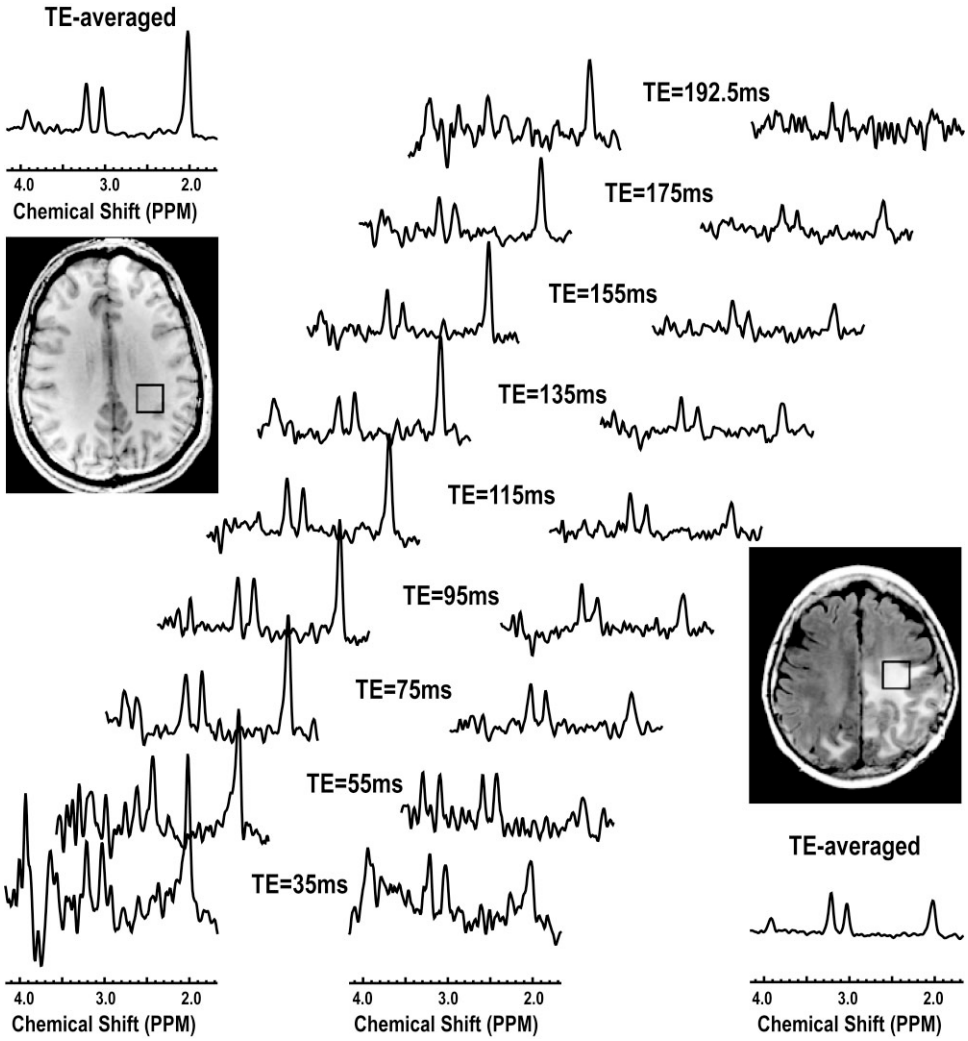

Figure 3. Single-voxel 2D J-resolved spectra acquired from a volunteer and a patient with a GBM. The TE-averaged spectra were plotted along the individual echo spectra.

was no movement between the image and spectra acquisition. The FLAIR image was aligned to the corresponding 3D SPGR image. Segmentation of the brain images was performed automatically on the 3D SPGR images using a program that is based on a Markov random field model (18). The segmented WM mask was then used to identify voxels that had at least 75% NAWM. The masks of the region of T_2 hyperintensity were segmented using a region-growing segmentation tool (19). The tumor voxels used for the study were restricted to those that were more than 80% within the T_2 hyperintensity. These were the voxels used for comparative analysis to the volunteer and patient data.

Statistics

The statistical analysis was performed using the SPSS software package (Chicago, IL, USA). A P value of <0.05 was regarded as significant for all the tests. For T_1 studies, nonparametric Wilcoxon rank sum tests were used to test the difference between lesions and normal tissues.

Analysis of variance (ANOVA) was utilized to determine whether T_2 values and metabolite levels differed between normal, grade 3, and grade 4. To check possible confounding effects of age and sex, these variables were added into the model. However, they did not change the effects of tumor grade and they were insignificant. And then Tukey's honestly significant difference tests were used to test these differences between tumor grades or between T_2 hyperintensity lesion and normal WM.

The Spearman rank correlation coefficients were calculated to determine the association between the estimated metabolite concentrations of LCModel and QUEST for Cho, Cr, and NAA after corrections with T_1 and T_2 relaxation times.

Changes of metabolite ratios by corrections with T_1 and T_2 relaxation times in each grade and overall were tested using a paired t-test, then a t-test was used to compare whether the effect of change was dependent on tumor grade.

RESULTS

The quality of data for the single-voxel data was excellent. Figure 3 shows an example of the 2D J-resolved and TE-averaged spectra from a volunteer and a patient. Note the differences in metabolite levels, with a clear reduction in the level of NAA in the voxel from tumor. At the shorter TEs peaks corresponding to Gln, Gln, and mI can be observed.

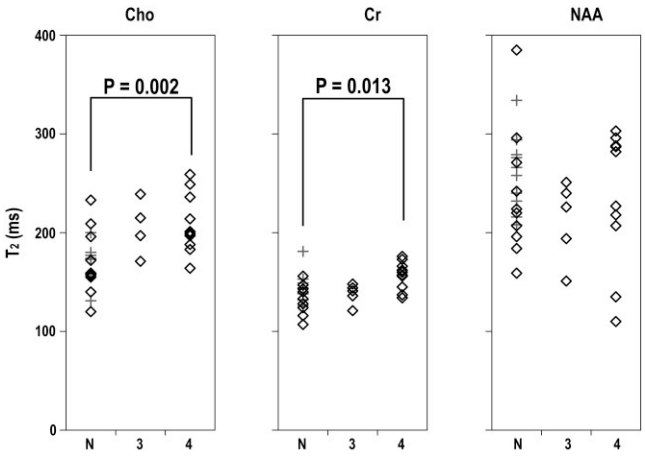

	Cho	Cr	NAA
Normal	169 ± 27	139 ± 16	249 ± 53
G3	199 ± 29	138 ± 10	212 ± 40
G4	209 ± 30	157 ± 14	235 ± 69

Figure 4. T_2 relaxation times for metabolites (msec). The significance was tested between normal WM and tumor using Tukey's honestly significant difference test. The diamond in the figure stands for data from patients, while the cross for volunteers. N, 3, and 4 represent values from WM in volunteers, and NAWM in patients with grade 3 and grade 4 lesions, respectively.

Metabolite T_1 Relaxation Times

The T_1 relaxation times of metabolites were available for voxels in eight volunteers and eight patients. Values were 1.06 ± 0.11 seconds (mean ± SD) vs. 1.00 ± 0.21 seconds for Cho, 1.38 ± 0.13 seconds vs. 1.37 ± 0.20 seconds for Cr, and 1.38 ± 0.13 seconds vs. 1.38 ± 0.21 seconds for NAA. There was no significant difference between these values.

Metabolite T_2 Relaxation Times

For the estimation of T_2 values, there were 10 voxels in WM from volunteers, three voxels from NAWM in patients with grade 3 glioma, and seven voxels from NAWM in patients with grade 4 glioma. Neither the values in WM and NAWM or their SDs were significantly different. The results were therefore pooled as normal WM VOIs for comparison with tumor voxels. NAWM voxels from patients were treated as independent observations from the values determined in the lesions because they were selected to be clearly distinct from the lesions on T_2-weighted images and did not appear to be correlated with tumor values. The pooled WM values for Cho were 169 ± 27 msec, for Cr were 139 ± 16 msec, and for NAA were 249 ± 53 msec. There were tumor voxels from five different patients with grade 3 glioma and 10 different patients with grade 4 glioma. The variations in T_2 relaxation values of metabolites for normal WM and patients were shown in Fig. 4. The range of NAA T_2 values was quite large, and they were not significantly different between normal WM and tumor voxels. For voxels from grade 3 glioma the T_2 values of Cho were 199 ± 29 msec but the small sample size meant that this was not significant. For voxels from grade 4 glioma the T_2 values of Cho were 209 ± 30 msec and for Cr were 1.57 ± 14 msec. These were significantly different from the values in normal WM with $P = 0.002$ and $P = 0.013$, respectively.

Metabolite Levels Corrected for Relaxation Times

Examples of TE-averaged spectra from normal parietal WM, grade 3 glioma, and grade 4 glioma that were quantified by LCModel and QUEST and are shown in Fig. 5. Both algorithms fit the data well, with the differences in the plotted spectra being due to the way in which the baseline estimation is performed. Because of the different relaxation times of metabolites in the basis sets for the two methods, due to one being simulated and the other from in vitro phantoms, the comparison between them only considered Cho, Cr, and NAA, which were corrected for T_1 and T_2 values. The fact that the estimates for Cho, Cr, and NAA obtained using LCModel and QUEST were consistent is reflected in Fig. 6. The Spearman rank correction coefficients were 0.92, 0.96, and 0.97 for Cho, Cr, and NAA estimates, respectively, with $P < 0.001$ for all three metabolites.

The estimates of metabolite levels obtained using QUEST and LCModel are further illustrated in Tables 1 and 2. Cho and Cr were clearly increased in grade 3 gliomas but decreased in grade 4 gliomas relative to normal brain. The differences in Cr between grades 3 and 4 lesions were statistically significant ($P < 0.01$). The concentrations of NAA were reduced in both tumor grades ($P < 0.001$). Compared with those in normal WM, the levels of mI estimated using LCModel were increased in grade 3 gliomas ($P = 0.002$) and statistical significantly different from grade 4 ($P = 0.017$). No significance was found for the results using QUEST. The

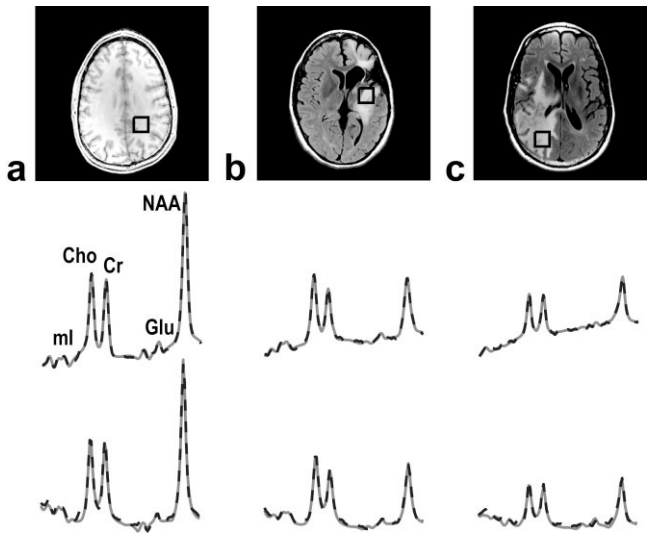

Figure 5. TE-averaged spectra quantified by LCModel (middle row) and QUEST (third row) corresponding to the image in a volunteer (**a**), grade 3 (**b**), and grade 4 (**c**) patients. The fitted spectra (straight line) were related to the phased spectra (broken line).

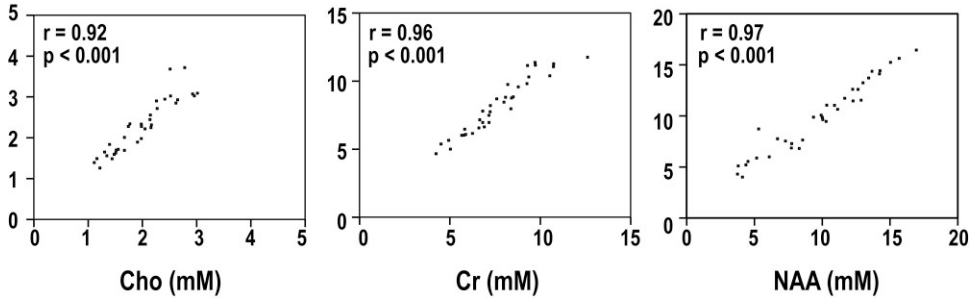

Figure 6. Scatter plots of Cho, Cr, and NAA calculated from LCModel vs. QUEST for all the voxels in the study. Metabolite concentrations on the x-axis represent those determined from LCModel, while the values on the y-axis were obtained from the same spectra using quantification by QUEST. The *P*-value represents the significance test for the correlation coefficient.

levels of Glu were significantly increased in grade 3 from QUEST ($P = 0.047$), and the difference between grade 3 and grade 4 for Gln was marginally significant for LCModel ($P = 0.05$).

Differences in Metabolite Ratios With and Without Corrections for T_2

Since the time available for data acquisition is relatively short in the case of in vivo MRSI data, the difference in T_2 relaxation times may contribute to the distinction between tumor and normal tissue. To investigate the magnitude of this effect, we considered the differences in metabolite ratios for our single-voxel data with and without correction for relaxation times. The metabolite ratios with and without corrections of relaxation values were shown in Table 3. In all cases, the Cho/Cr, NAA/Cr, and Cho/NAA ratios in tumors were larger than in normal WM for the uncorrected compared to the corrected values. This implies that the differential in relaxation times between Cho, Cr, and NAA increases the contrast for spectra in tumor relative to normal tissue when there is a higher degree of T_2-weighting. Statistical significance was found for the interaction between the correction and tumor grade for all the metabolite ratios with $P < 0.001$.

DISCUSSION

Gliomas are the most common primary brain tumor and primarily affect WM. The ability to map out the spatial extent of tumor relative to NAWM is dependent upon both the variations in absolute concentrations of metabolites and in degree of T_1- and T_2-weighting in any given acquisition. Designing the most appropriate acquisition parameters for obtaining multivoxel MRSI data requires the measurement of these variables in localized spectra from normal volunteers and patients with brain tumors.

The methods used in this study to estimate relaxation times and metabolite levels had several benefits over previous approaches. First, the individual spectra that used for T_2 fitting were the mean of three spectra with a TE difference of 2.5 msec, which increased the SNR, as shown in Fig. 3. This can be expected to provide more reliable estimates of the T_2 values. Note that J-coupling

Table 1
Concentrations of Cho, Cr, and NAA as Corrected Using Empirical T_1 and T_2 Relaxation Times and Expressing the (Mean ± SD) in mM by QUEST and LCMODEL*

Methods	Metabolite	Group	Concentrations	Population	G3	G4
QUEST	Cho	Normal	2.3 ± 0.5	$N = 20$		
		G3	2.9 ± 0.9	$N = 5$		$P < 0.01$
		G4	1.9 ± 0.5	$N = 10$	$P < 0.01$	
	Cr	Normal	8.9 ± 1.6	$N = 20$		$P < 0.001$
		G3	9.1 ± 2.4	$N = 5$		$P < 0.005$
		G4	6.0 ± 0.9	$N = 10$	$P < 0.005$	
	NAA	Normal	12.4 ± 2.1	$N = 20$	$P < 0.001$	$P < 0.001$
		G3	6.8 ± 1.5	$N = 5$		
		G4	6.3 ± 1.6	$N = 10$		
LCModel	Cho	Normal	2.0 ± 0.5	$N = 20$		
		G3	2.3 ± 0.6	$N = 5$		
		G4	1.7 ± 0.6	$N = 10$		
	Cr	Normal	8.4 ± 1.5	$N = 20$		$P = 0.001$
		G3	8.6 ± 2.6	$N = 5$		$P < 0.001$
		G4	5.8 ± 1.1	$N = 10$	$P < 0.001$	
	NAA	Normal	12.5 ± 2.1	$N = 20$	$P < 0.001$	$P < 0.001$
		G3	5.5 ± 1.5	$N = 5$		
		G4	6.6 ± 2.2	$N = 10$		

*Statistics were evaluated using Tukey's honestly significant difference tests.
N = number of patients.

Table 2
Levels of mI, mIG, Glu, and Gln as Quantified by QUEST and LCModel (Mean ± SD)*

Methods	Metabolite	Group	Levels	Population	G3	G4
QUEST	mI	Normal	2.8 ± 0.9	$N = 20$		
		G3	3.8 ± 1.2	$N = 5$		
		G4	2.8 ± 1.7	$N = 8$		
	mIG	Normal	3.6 ± 1.1	$N = 20$		
		G3	5.1 ± 1.8	$N = 5$		
		G4	3.3 ± 1.6	$N = 8$		
	Glu	Normal	2.3 ± 0.5	$N = 14$	$P < 0.05$	
		G3	3.1 ± 0.8	$N = 4$		$P < 0.05$
		G4	2.1 ± 0.5	$N = 4$	$P < 0.05$	
	Gln	Normal	2.5 ± 0.9	$N = 19$		
		G3	2.7 ± 0.1	$N = 2$		
		G4	2.3 ± 0.7	$N = 9$		
LCModel	mI	Normal	5.9 ± 1.5	$N = 14$	$P < 0.005$	
		G3	10.4 ± 2.4	$N = 4$		$P < 0.05$
		G4	6.4 ± 2.7	$N = 5$	$P < 0.05$	
	Glu	Normal	6.3 ± 1.9	$N = 14$	n/a	
		G3	8.4	$N = 1$		
		G4	5.4 ± 1.5	$N = 3$	n/a	
	Gln	Normal	2.2 ± 0.3	$N = 3$		
		G3	2.4 ± 0.6	$N = 4$		$P = 0.05$
		G4	1.5 ± 0.5	$N = 5$	$P = 0.05$	

*Statistics were evaluated using Tukey's honestly significant difference tests.
N = number of patients.

differences within these three averaged spectra would have been very small and were therefore ignored. The second benefit in using the 2D refocused sequence is that the effective TE was relatively long, and would therefore reduce the effects of macromolecules and decrease the contribution of J-coupled resonances of Glu located underneath the NAA peak. Although the last echo in the T_2 fit (TE = 190 msec) was not long enough to cover the complete signal decay, more points were involved in our study than in previous publications (20–22). Third, since the TE-averaged spectra had a flat baseline, the possibility of overestimating T_1 values should be relatively small.

A limitation of the approach used was that the weak signal intensities of Glu and mI translated into a large variation and uncertainty in peak intensities for individual TEs and so the T_1 and T_2 of these metabolites were not able to be evaluated. To estimate the T_2 values of metabolites such as mI, Glu, and Gln with complex J-coupling patterns would require a metabolite-specific spectral editing sequence (23,24).

Several studies have assessed the T_1 and T_2 relaxation times of normal brain metabolites within different regions of the normal brain and at different field strengths. T_1 values were significantly longer at 3T than at 1.5T (21), but were not reported as showing major regional variability (22). A distinct correlation was reported between T_2 and relative WM/gray matter (GM) composition for NAA and Cr-CH_3 (22). This suggests that the T_2 of these intracellular metabolites is more affected by the integrity and composition of the tissue, whereas T_1 values are influenced by molecular tumbling, reflecting the viscosity of the medium. The T_1 relaxation times of metabolites from normal brain that were observed in our study are similar to those previously published (22), and were not significantly different from the T_1 values in gliomas. While this is consistent with observations made at 1.5T (7) it may also be due to the limited number of cases in the study.

The T_2 relaxation times of metabolites from normal WM, including fourteen parietal WM and six frontal WM, in our study, are close to that previously published (9), which also investigated T_2 values in the parietal WM. T_2 relaxation times in Cho and Cr were statistically significantly longer in grade 4 gliomas compared with those in normal WM. The Cho peak resonates at 3.20 ppm and represents choline, phosphocholine (PC), and glycerophosphocholine (GPC). Previous studies have shown that a switch from GPC to PC is associated with glioma malignancy (25,26). This could be one reason

Table 3
Relative Metabolite Ratios (Mean ± SD)*

	Cho/Cr		NAA/Cr		Cho/NAA	
	Uncorrected	Corrected	Uncorrected	Corrected	Uncorrected	Corrected
Normal	0.36 ± 0.05	0.24 ± 0.03	1.84 ± 0.23	1.51 ± 0.19	0.20 ± 0.04	0.16 ± 0.03
G3	0.47 ± 0.13	0.28 ± 0.08	0.80 ± 0.37	0.71 ± 0.33	0.70 ± 0.35	0.47 ± 0.23
G4	0.46 ± 0.09	0.29 ± 0.06	1.23 ± 0.35	1.14 ± 0.33	0.42 ± 0.23	0.29 ± 0.16

*The ratios of Cho/Cr, NAA/Cr, and Cho/NAA estimated by LCModel were compared with the same data after the corrections of T_1 and T_2 values.

why the observed T_2 of Cho increases in tumor. The higher T_2 of Cr in grade 4 glioma may also be associated with the changes of metabolite composition, associated with the increase of phosphocreatine (PCr) to Cr. Note that PCr contains a high-energy phosphate bond, which transfers to adenosine diphosphate (ADP) via the breakdown of PCr to Cr and that reduced PCr has been observed in gliomas (27). This suggests that there is a high energy requirement for maintaining the growth of cells in gliomas. In the previous studies that were performed at 1.5T, either the T_2 relaxation time of NAA and Cr were reported to be shorter in high-grade gliomas (6) or the T_2 relaxation time of all of the singlets were shorter in the tumor (7). The differences observed in our study may be because of the higher field strength used, the larger number spectra employed in calculating the T_2 values, or the application of a more effective statistic test, Tukey's honestly significant difference test, instead of a regular Student's *t*-test. Compared to Bonferroni correction, which is known to be overly conservative in the adjustment of multiple comparisons, Tukey's honestly significant difference test takes into account the correlation structure of the ANOVA model and is more efficient.

The elevation of the Cho peak and the reduction of the neuronal marker NAA are considered to be characteristic of gliomas. Our results suggest that the changes in Cho and Cr peak heights in gliomas are partially caused by T_2 effects and partially by changes in absolute concentrations, and that a significant interaction exists between corrections for relaxation times and tumor grade. Longer T_2 relaxation value of Cho in gliomas means that the ratio of Cho/NAA that is observed in long echo spectra is larger than that in short echo spectra and relatively larger than values in normal WM at the same TE. This is consistent with the previous observations at 1.5T (28).

Two different algorithms were used to quantify the metabolic profiles in our study. LCModel uses a constrained regularization method accounting for the phase, lineshape, and baseline (12). QUEST differs from the LCModel in the method used for fitting the baseline, and is sensitive to whether a common extra damping factor or different metabolite extra damping is estimated (13). In our case, we used a simulated basis set and found better results when a unique common extra damping was estimated. Since there is little penalty for the contamination of macromolecules and lipids in the TE-averaged spectra (8,9,29), we used the QUEST quantification algorithm without background adjustment, but weighted the first 20 points with a quarter-wave sinusoid and discarded the first points to reduce the influence of broad resonances underlying metabolites of interest. The results of the estimates of Cho, Cr, and NAA showed a very high correlation coefficient between the two methods. Compared with LCModel, QUEST gives more flexibility and reliability but has more subjective interaction, which requires the use of more prior knowledge.

As expected, there was a striking reduction in NAA for all the grades of glioma. The higher metabolite levels in grade 3 compared to grade 4 glioma suggested that the levels in the higher-grade lesions may be influenced by partially voluming with necrosis (30). The mI is predominantly located within astrocytes and is a precursor for the phosphatidylinositol (PI) second-messenger system (31) that is also presumed to act as an osmoregulator. It resolves as an apparent doublet at 3.6 ppm in TE-averaged spectra, which cannot be separated from the Gly peak that resonates at 3.56 ppm. Compared to the simulation, the doublet of mI from the in vitro solution had different effective T_2 values, which resulted in the difference of fitting outcomes between LCModel and QUEST. Changes that are associated with mI and reported in the literature show increases in mIG (32) and its ratio to Cr (33) in low-grade astrocytomas but decreased in high-grade. In our results, the mI estimated from LCModel was statistically significantly higher in grade 3 compared to normal WM.

Although averaged 2D J-resolved spectra have less macromolecule contamination compared with short-echo acquisitions, macromolecules are always associated with gliomas and result in more uncertainty of small peaks such as Glu/Gln. The changes observed with LCModel and QUEST had a similar pattern of changes. Previous studies have showed that a significant increase in Glu/Gln (Glx) was found in oligodendrogliomas and was used to discriminate them relative to low-grade astrocytomas (34). The increase in Glu that was observed in the grade 3 glioma considered in our study is consistent with the observation that glioma cells may secrete Glu, resulting in an increase in extracellular Glu (35,36). Increased Glu could be also associated with inflammation in the peritumor tissues since activated microglia and brain macrophages express high-affinity Glu transporters (37) and stimulate tumor cell proliferation. Gln was also slightly increased in grade 3 but the change was not statistically significant. Because Gln acts as an suppressor for apoptosis, it could contribute to block apoptosis induced by exogenous agents, such as radiation treatment and chemotherapy, and also promote tumor proliferation (38). As predicted by the simulation, the signal intensities of Glu and Gln in the TE-averaged spectra depend on the T_2 values. The pattern of changes in Gln for gliomas would be much clearer if estimates of the T_2 of Glu and Gln were obtained. Although mobile lipids and lactate (Lac) are also strongly associated with the higher grade of gliomas, it was not possible to distinguish Lac from lipid in the TE-averaged spectra. It is for this reason that we did not attempt to quantify these metabolites in the current study.

It is well known that gliomas are extremely heterogeneous. The regions of T_2 hyperintensity on the T_2-weighted image may include edema, gliosis, inflammation, active tumors, or treatment effects. While we chose to consider large tumors and required that 80% of the voxel considered be in the tumor, the effect of heterogeneity is a limitation in terms of the results of our study. Due to the large voxel size in the study (8-cc), it was not possible to evaluate the differences between enhancing and nonenhancing lesions. This would require multivoxel acquisitions (39). Obtaining biopsies from the region with the highest metabolite ratio (Cho/NAA) may further help to understand the underlying biologic characteristics of the tumor. Another factor

that may have influenced the data is that there were four different grades of gliomas considered, which arise from different glial cells, such as oligodendrocytes and astrocytes, and could therefore result in different metabolite characterizations (34).

In conclusion, the results of our study demonstrated the differences in metabolite relaxation times and in metabolite concentrations both between normal WM and tumor and between glioma of grade 3 and grade 4. These data suggest that the contrast in metabolite rations between tumor and normal tissue would be greatest at longer TEs and, if the SNR is high enough, the use of long TEs may have benefits over short TEs. Our results are encouraging but further studies are required to provide more information about the spatial variations in metabolite concentrations within tumor and peritumor regions using multivoxel acquisitions in populations of patients with gliomas.

REFERENCES

1. Gill SS, Thomas DG, Van Bruggen N, et al. Proton MR spectroscopy of intracranial tumours: in vivo and in vitro studies. J Comput Assist Tomogr 1990;14:497–504.
2. Fulham MJ, Bizzi A, Dietz MJ, et al. Mapping of brain tumor metabolites with proton MR spectroscopic imaging: clinical relevance. Radiology 1992;185:675–686.
3. Preul MC, Caramanos Z, Collins DL, et al. Accurate, noninvasive diagnosis of human brain tumors by using proton magnetic resonance spectroscopy. Nat Med 1996;2:323–325.
4. Tong Z, Yamaki T, Harada K, Houkin K. In vivo quantification of the metabolites in normal brain and brain tumors by proton MR spectroscopy using water as an internal standard. Magn Reson Imaging 2004;22:1017–1024.
5. Li Y, Osorio JA, Ozturk-Isik E, et al. Considerations in applying 3D PRESS H-1 brain MRSI with an eight-channel phased-array coil at 3 T. Magn Reson Imaging 2006;24:1295–1302.
6. Isobe T, Matsumura A, Anno I, et al. Quantification of cerebral metabolites in glioma patients with proton MR spectroscopy using T2 relaxation time correction. Magn Reson Imaging 2002;20:343–349.
7. Sijens PE, Oudkerk M. 1H chemical shift imaging characterization of human brain tumor and edema. Eur Radiol 2002;12:2056–2061.
8. Hurd R, Sailasuta N, Srinivasan R, Vigneron DB, Pelletier D, Nelson SJ. Measurement of brain glutamate using TE-averaged PRESS at 3T. Magn Reson Med 2004;51:435–440.
9. Srinivasan R, Sailasuta N, Hurd R, Nelson S, Pelletier D. Evidence of elevated glutamate in multiple sclerosis using magnetic resonance spectroscopy at 3 T. Brain 2005;128:1016–1025.
10. Wright SM, Wald LL. Theory and application of array coils in MR spectroscopy. NMR Biomed 1997;10:394–410.
11. Young IR, Bailes DR, Burl M, et al. Initial clinical evaluation of a whole body nuclear magnetic resonance (NMR) tomograph. J Comput Assist Tomogr 1982;6:1–18.
12. Provencher SW. Estimation of metabolite concentrations from localized in vivo proton NMR spectra. Magn Reson Med 1993;30:672–679.
13. Ratiney H, Sdika M, Coenradie Y, Cavassila S, van Ormondt D, Graveron-Demilly D. Time-domain semi-parametric estimation based on a metabolite basis set. NMR Biomed 2005;18:1–13.
14. Knijn A, de Beer R, van Ormondt D. Frequency-selective quantification in the time domain. J Magn Reson 1992;97:444–450.
15. Pijnappel WWF, van den Boogaart A, de Beer R, van Ormondt D. SVD-based quantification of magnetic resonance signals. J Magn Reson 1992;97:122–134.
16. Smith SA, Levante TO, Meier BH, Ernst RR. Computer simulations in magnetic resonance. An object-oriented programming approach. J Magn Reson 1994;106:75–105.
17. Govindaraju V, Young K, Maudsley AA. Proton NMR chemical shifts and coupling constants for brain metabolites. NMR Biomed 2000; 13:129–153.
18. Zhang Y, Brady M, Smith S. Segmentation of brain MR images through a hidden Markov random field model and the expectation-maximization algorithm. IEEE Trans Med Imaging 2001;20:45–57.
19. Saraswathy S, Crawford F, Nelson SJ. Semi-automated segmentation of brain tumor lesions in MR images. In: Proceedings of the 14th Annual Meeting of ISMRM, Seattle, WA, USA, 2006 (Abstract 1609).
20. Mlynarik V, Gruber S, Moser E. Proton T (1) and T (2) relaxation times of human brain metabolites at 3 Tesla. NMR Biomed 2001; 14:325–331.
21. Ethofer T, Mader I, Seeger U, et al. Comparison of longitudinal metabolite relaxation times in different regions of the human brain at 1.5 and 3 Tesla. Magn Reson Med 2003;50:1296–1301.
22. Traber F, Block W, Lamerichs R, Gieseke J, Schild HH. 1H metabolite relaxation times at 3.0 Tesla: measurements of T1 and T2 values in normal brain and determination of regional differences in transverse relaxation. J Magn Reson Imaging 2004;19:537–545.
23. Choi C, Coupland NJ, Bhardwaj PP, et al. T2 measurement and quantification of glutamate in human brain in vivo. Magn Reson Med 2006;56:971–977.
24. Choi C, Coupland NJ, Bhardwaj PP, Malykhin N, Gheorghiu D, Allen PS. Measurement of brain glutamate and glutamine by spectrally-selective refocusing at 3 Tesla. Magn Reson Med 2006;55: 997–1005.
25. Usenius JP, Vainio P, Hernesniemi J, Kauppinen RA. Choline-containing compounds in human astrocytomas studied by 1H NMR spectroscopy in vivo and in vitro. J Neurochem 1994;63:1538–1543.
26. Aboagye EO, Bhujwalla ZM. Malignant transformation alters membrane choline phospholipid metabolism of human mammary epithelial cells. Cancer Res 1999;59:80–84.
27. Negendank W. Studies of human tumors by MRS: a review. NMR Biomed 1992;5:303–324.
28. Kaminogo M, Ishimaru H, Morikawa M, et al. Diagnostic potential of short echo time MR spectroscopy of gliomas with single-voxel and point-resolved spatially localised proton spectroscopy of brain. Neuroradiology 2001;43:353–363.
29. Bolan PJ, DelaBarre L, Baker EH, et al. Eliminating spurious lipid sidebands in 1H MRS of breast lesions. Magn Reson Med 2002;48: 215–222.
30. Kinoshita Y, Yokota A. Absolute concentrations of metabolites in human brain tumors using in vitro proton magnetic resonance spectroscopy. NMR Biomed 1997;10:2–12.
31. Kofman O, Belmaker RH. Ziskind-Somerfeld Research Award 1993. Biochemical, behavioral, and clinical studies of the role of inositol in lithium treatment and depression. Biol Psychiatry 1993; 34:839–852.
32. Howe FA, Barton SJ, Cudlip SA, et al. Metabolic profiles of human brain tumors using quantitative in vivo 1H magnetic resonance spectroscopy. Magn Reson Med 2003;49:223–232.
33. Castillo M, Smith JK, Kwock L. Correlation of myo-inositol levels and grading of cerebral astrocytomas. AJNR Am J Neuroradiol 2000;21:1645–1649.
34. Rijpkema M, Schuuring J, van der Meulen Y, et al. Characterization of oligodendrogliomas using short echo time 1H MR spectroscopic imaging. NMR Biomed 2003:16:12-18.
35. Takano T, Lin JH, Arcuino G, Gao Q, Yang J, Nedergaard M. Glutamate release promotes growth of malignant gliomas. Nat Med 2001;7:1010–1015.
36. Ye ZC, Ransom BR, Sontheimer H. (1R,3S)-1-Aminocyclopentane-1,3-dicarboxylic acid (RS-ACPD) reduces intracellular glutamate levels in astrocytes. J Neurochem 2001;79:756–766.
37. Piani D, Frei K, Do KQ, Cuenod M, Fontana A. Murine brain macrophages induced NMDA receptor mediated neurotoxicity in vitro by secreting glutamate. Neurosci Lett 1991;133:159–162.
38. Mates JM, Perez-Gomez C, Nunez de Castro I, Asenjo M, Marquez J. Glutamine and its relationship with intracellular redox status, oxidative stress and cell proliferation/death. Int J Biochem Cell Biol 2002;34:439–458.
39. Li Y, Chen AP, Crane JC, Chang SM, Vigneron DB, Nelson SJ. Three-dimensional J-resolved H-1 magnetic resonance spectroscopic imaging of volunteers and patients with brain tumors at 3T. Magn Reson Med 2007;58:886–892.